ISSN (Print 0974-2115) (Online 2349-8552)
www.jchps.com Journal of Chemical and Pharmaceutical Sciences

Fabrication a solar cell by synthesize a new nano particles of Quinoline derivative and its metal complex with studing the optical, structural and morphological properties

[1]Ahmad H. Ismail, [2]Ahmed N. Abd, [3]Hayder K. Kareem*
[1]Department of Chemistry, College of Science, University of Al-Mustansiriya, Baghdad, Iraq
[2]Department of Physics, College of Science, University of Al-Mustansiriya, Baghdad, Iraq
[3]Ministry of Education, Al-kerakh/3 Education General Management
***Corresponding author: E-Mail: Haidermalkey@yahoo.com**

ABSTRACT

In this paper, Nanoparticles thin films of (E)-1-((benzo[d][1,3]dioxol-5-ylmethylene)amino)quinolin-2(1H)-one)(L) and its complex have been prepared as a novel compounds. The prepared compounds have been applied in Fabrication of solar Cell.

The ligand (L) was synthesized from the reaction of N-amino quinoline-2-one with piperonaldehyde. N-amino quinoline-2-one (S) as starting material was prepared by the refluxing reaction of coumarin with hydrazine hydrate in ethanolic media (99%) for 12 hours. The synthesized ligand was characterized by using (FT-IR), (U.V-Vis), (^{1}H NMR) spectra, as well as melting point and (C.H.N) elemental analysis. The metal complex (M) was obtained by the stoichiometry molar ratio (2:1) (L:M). The prepared complex was diagnosed by magnetic susceptibility measurements, molar conductivity and spectroscopic methods, i.e., [FT-IR, UV-Vis, more over the Atomic Absorbance technique]. According to the obtained results from the different techniques in above an octahedral geometry has been suggested for the prepared complex, And then the prepared compounds have been precipitated on the glass substrates to achieve the thin films using the drop casting method. The structural, optical and morphology properties have been studied and then precipitated on the silicon slides so as to fabrication of a solar cell with development its properties.

KEY WORDS: Coumarin, quinoline, Schiff base, Transition Metal (Ii) Complex, Solar Cell.

1. INTRODUCTION

Green chemistry is one of the important economic and environmental solutions of rapid pollution growth, which produce from using fossil fuels and other usual energies . Although it has been predicted that fossil fuels will drain away within 100 years. recently, the trend toward the renewable energy resources become urgent necessary so as to override the pollution risks . The light of the sun is abundant, reliable, free, and uniformly distributed energy resource, therefor is use as a save energy in green chemistry reactions (Ali, 2016).

Heterocyclic compounds can be used to increase the solar cell efficiency which can be used as electron acceptors to produce a photocurrent (Zheng, 2016). Coumarin compound is the basic part in various natural products (Witaicenis, 2014), which can be used as starting material to production the quinolone compound (Jennifer, 2014). The quinolone compounds have photoelectrical activity (Xi, 2015), so it could be used in laser devices, fluorescent probes and light-emitting diodes because it's have good optical properties(Luo, 2015). A lot of quinoline complexes can be used in fabrication of solar cell due to the absorption of sun light in the visible region, lower cost and low toxicity (Huang, 2016).

The present research report the preparations of new Nanoparticles compounds with characterization and study of optical, structural and Morphology properties of N-amino quinoline-2-one derivative and complex with Cu(II) ion. The synthesized compounds used in Fabrication solar cell and found both of fill factor and efficiency for it.

2. EXPERIMENTAL

Materials and Methods: The chemical materials used in the work are reagent grade (supplied by either Fluka or Merck) and used without further purification. Melting points were recorded by using SMP30 melting point apparatus. ^{1}H NMR spectra were recorded using Bruker DMX-500 (300 M Hz) and d^6–DMSO as a solvent at University of Al- Albayt, Amman, Jordan. Infrared spectra of the prepared compounds were recorded as (KBr) disc by using shimadzu,(4800S)(FTIR) spectrophotometer in the range (4000-400)cm^{-1}. Electronic spectra of the prepared compounds were obtained by using (U.V-Vis) spectrophotometer type Cary 100 con at range (200-900) nm. Magnetic susceptibility measurement for complex was obtained by using Balance Magnetic susceptibility, Model(MSB-MK1). Elemental micro analysis for the ligand was performed on a (C.H.N)analyzer from EURO EA (EA3000) elemental analyzer. Metal content of the complex was determined by atomic absorption (A.A) technique, using a phoenix-986 AA spectrophotometer. Electrical conductivity measurement of the complex was recorded at (25°C) for (10^{-3} M) solution of the complex in DMSO by using an Inolap Multi 740,WTW 82362 Weilhiem-Germany.

X-ray diffractometer (XRD-6000, Shimadzu). Optical microscope (Leice dm 2500p). Atomic force microscope AFM (AA 3000 scanning probe microscope).

Synthesis of starting material (Abid, 2016): N-amino quinoline-2-one (S) was prepared by Refluxing of coumarin (7.3 g, 0.05 mole) with hydrazine hydrate 99% (25 g, 0.5 mole) in 30 ml absolute ethanol for 12 hours, scheme.1. The obtained Light yellow precipitate washed with absolute ethanol, then dried and recrystallized by using ethanol solvent to get a pure sample, yield: 92%, M.P.(131 – 133°C). M.Wt.(160 g.mole^{-1}) with general formula ($C_9H_8N_2O$). Elemental analysis, theoretical (%) C (67.5), H (5), N (17.5); experimental (%) C (67.37), H (5.28), N (17.41), have shown in table.1.

Synthesis of Schiff base: The Schiff base ligand (L) was prepared by condensation reaction (1.6 g, 0.01mole) of N-amino quinoline-2-one and (1.5 g, 0.01mole) piperonaldehyde, Few drops of glacial acetic acid was added as catalyst, in absolute ethanol 25 ml and refluxed for 7 hours, scheme.1. The obtained yellow precipitate washed several times with absolute ethanol, then dried and recrystallized from ethanol to get a pure sample, yield: 78%, M.P.(179 – 181°C), M.Wt. (292 g.mole^{-1}) and general formula ($C_{17}H_{12}O_3N_2$). Elemental analysis, theoretical (%) C (69.86), H (4.11), N (9.59); experimental (%) C (69.75), H (4.34), N (9.49), table.1.

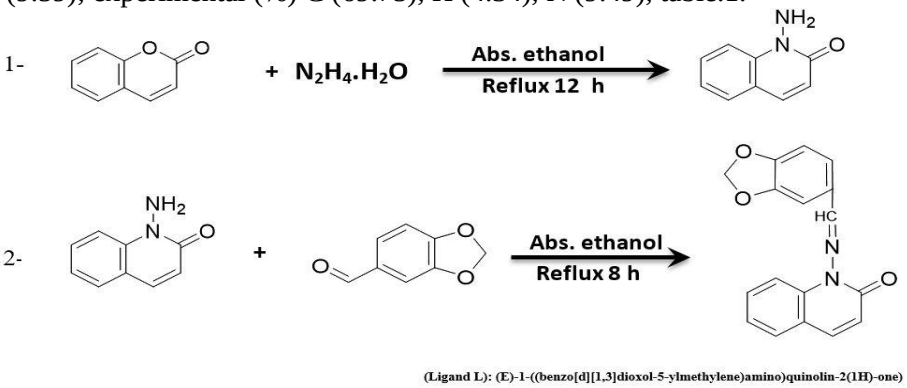

Scheme.1. The Synthesis route of ligand (L)

Synthesis of metal complex(M): An ethanolic solution Contenting (0.584 g, 2m mole) of ligand (L) with (0.17 g, 1m mole) of $CuCl_2.2H_2O$ in (2:1) (L:M) molar ratio, were refluxed with continuous stirring for 4 hours. The resulting mixture was filtered and washed with an excess of ethanol, then dried and recrystallized by a mixture from distilling water with DMSO (3:7) to get a pure sample. A green solid was obtained, yield 71%, M.P. (200-202°C), M.Wt.(718.4 g.mole^{-1}). The physical properties of the metal complex are listed in table.1.

Table.1. The Microanalysis results and Some physical properties of the starting material, ligand and metal complex

Symbol	General formula	Molecular weight (g/mole)	M.P C°	Yield %	Color
S	$C_9H_8N_2O$	160	131–133	92%	Light yellow
L	$C_{17}H_{12}O_3N_2$	292	179-181	78%	Yellow
M	$[CuL_2Cl_2]$	718.4	200-202	71%	Green

Theoretical (exp.)				
Symbol	**C%**	**H%**	**N%**	**M%**
S	67.5 (67.37)	5 (5.28)	17.5 (17.41)	------
L	69.86 (69.75)	4.11 (4.34)	9.59 (9.49)	------
M	------	------	------	8.84 (9.04)

Thin films deposition by drop casting method: Glass slides of (1.0 x1.5) cm^2 area, were used as a substrate. They were cleaned with absolute ethanol to remove the impurities and residuals from their surface. Five drops of the colloidal were used in preparing the (L and M) thin films on glass by drop casting method (Majeed, 2015). Silicon wafer was chemically etched in a dilute Hydrofluoric acid (HF) in or order to remove native oxides then the wafers were cut into pieces with a dimension of (1.5 × 1.5) cm^2. The back side of the wafer was deposited with 1µm thick aluminum back contact using thermal evaporation technique at (10^{-5}) torr vacuum (Abd, 2015).

3. RESULTS AND DISCUSSION

^{1}HNMR spectra: The ^{1}HNMR spectrum of ligand was found to agree with the number of different types of protons present. The formation of Schiff base is supported by the presence of a singlet signal at δ (8.6) ppm corresponding to the azomethine proton (–N=CH–). The multiplied signals of the aromatic protons were assigned in range δ (7.02-7.42) ppm. The peaks were appeared as singlet at δ (6.1) ppm attributed to (-CH_2) group (Alaghaz, 2013), figure.1.

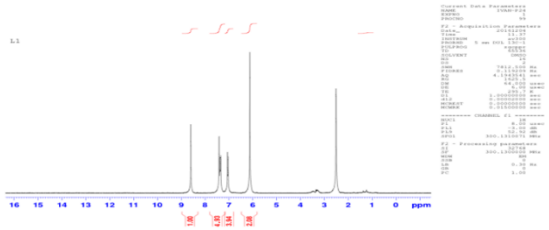

Figure.1. The ^{1}HNMR spectra of ligand (L)

FT-IR spectra: The (FT-IR) spectrum of piperonaldehyde exhibits a strong band due to the stretching vibration of υ(C=O)group which appears at (1682)cm^{-1}. The compound N-amino quinoline-2-one (S) exhibits two bands at (3298,3286) cm^{-1} are due to the asymmetric and symmetric stretching vibrations of the primary amine (NH_2).

A strong band which appears at (1639)cm^{-1} is due to the stretching vibration of carbonyl amide group, while the bands at (1593,1450) cm^{-1} and (3051)cm^{-1} were assigned to the stretching vibration of υ(C=C) and υ(C-H) aromatic, respectively (Kumar, 2014). The (FT-IR) spectrum of the ligand (L) displays a new band at (1622)cm^{-1} was assigned to the υ (HC=N-) stretching mode of vibration of the azomethine group with disappearance the band which Attributed to the stretching vibration of the primary amine in the compound (S), the (FT-IR) spectrum of the ligand records the stretching vibration band of carbonyl amid group at (1666)cm^{-1}. The bands at (2995)cm^{-1}, (3078)cm^{-1} and (1560)cm^{-1} were assigned to the stretching vibrations of υ(C-H)aliphatic, υ(C-H) aromatic and υ(C=C) aromatic respectively. The band at (1199)cm^{-1} is due to the stretching vibrations of υ(C-N) (Shakya, 2012), figure.2.

On complexation the band which appeared at (1622) cm^{-1} in the spectrum of ligand was shifted to lower frequency at (1589) cm^{-1} indicating the contribution of nitrogen azomethine group in coordination with metal ion . The stretching vibration band at (1666) cm^{-1} has been shifted to lower frequency (1629)cm^{-1} for complex, showing that the contribution the carbonyl amide group in coordination process through the Oxygen atom. In the lower frequency region the weak bands observed at (435) cm^{-1} and (578) cm^{-1} have been assigned, respectively, to the υ(M-O) and υ(M-N) vibrations (Kumar, 2014), figure.3.

Table.2. Major Infra – red absorption bands of starting materials, Ligand and complex (cm^{-1})

Compound	υ(NH_2)	υ(C=O)	υ(C=N)	υ(M-N)	υ(M-O)
Piperonaldehyde	-----	1682	-----	-----	-----
$C_9H_8N_2O$(S)	3298, 3286	1639	-----	-----	-----
$C_{17}H_{12}O_3N_2$(L)	-----	1666	1922	------	------
[Cu(L) $_2Cl_2$] (M)	-----	1629	1589	578	435

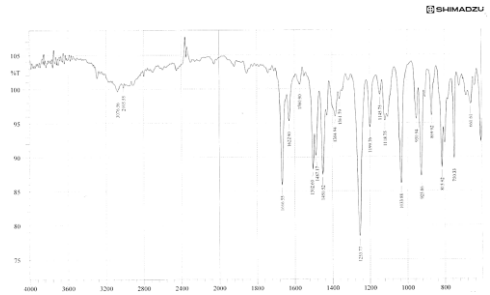

Figure.2. The FTIR spectrum of ligand(L)

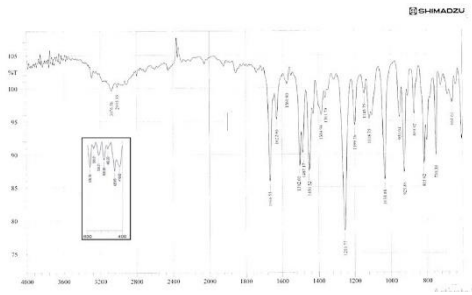

Figure.3. The FTIR spectrum of complex (M)

Electronic spectra: The electronic spectral study of ligand was carried out in DMSO (10^{-3} M) solution, exhibits tow high intense peaks at 248 nm (40322cm^{-1}) (ε_{max}=11152 molar^{-1}.cm^{-1}) and 292 nm (34246cm^{-1}) (ε_{max}=826 molar^{-1}. cm^{-1}) assigned to (π -π*) and (n - π*) electronic transitions within the organic ligand (Jayamani, 2014), figure.4. The copper (II) complex shows four peaks. Tow high intense peaks at 257 nm (38910 cm^{-1}) (ε_{max}=1040 molar^{-1}.cm^{-1}) and 312nm (32051 cm^{-1}) (ε_{max}=660 molar^{-1}.cm^{-1}) are due to (π -π*) and (n - π*) respectively, while the third peak at 346 nm (28901 cm^{-1}) (ε_{max}=405 molar^{-1}.cm^{-1}) is due to the charge transfer and the fourth (d-d) transition at 866nm (11547 cm^{-1}) (ε_{max}=53 molar^{-1}.cm^{-1}) is due to the ^{2}Eg ^{2}Tg transition, figure.5. The electronic spectral bands suggest an octahedral geometry around the cu(II) ion (Tyagi, 2014).

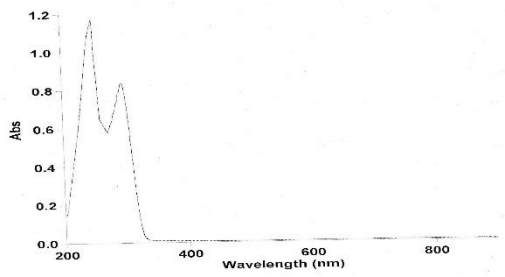

Figure.4. The electronic spectra of ligand (L)

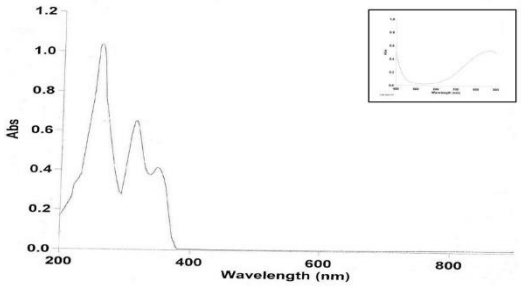

Figure.5. The electronic spectra of complex (M)

Magnetic susceptibility and conductivity: The magnetic moment of the Cu(II) d^9 (Term ^2D), exhibit normal magnetic moments (1.65 B.M.) which is in agreement with data reported by several research workers (Shebl, 2014). Electrical conductivity measurements of the complex were recorded at (25ºC) for (10^{-3}.L^{-1}) solution of the sample in DMSO, the complex behaved as non-electrolyte. The analytical data of the transition metal complex of the synthesized ligand confirmed a molar ratio (1:2) (M:L) as shown below in figure.6.

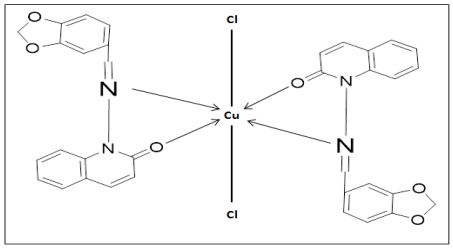

Figure.6. Suggested structure of Cu(II) complex

Structural properties: The XRD diffraction patterns of synthesized compounds (L and M) Nanoparticles films and deposited on glass substrates as shown eight and five peaks for L and M compounds, respectively,the resultant relive that both them are polycrystalit, Figure.7.

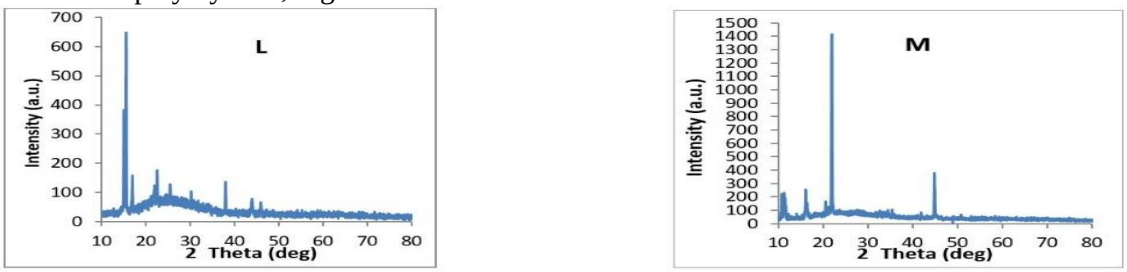

Figure.7. XRD patterns of (L and M) thin films

Table.3. shows the crystallite size ,micorstrain and dislocation density.

Table.3. characterization of XRD

Compound	2 Theta (deg)	β(deg)	D nm	microstrain x 10^{-4}	δ x 10^{-14} lines.m^{-2}
L	15.52	5.70	1.39	247.81	5114.89
	14.98	5.90	1.34	256.85	5495.16
	37.90	2.37	3.52	98.32	805.25
M	22.02	4.03	1.99	173.57	2509.52
	44.83	2.02	4.23	81.83	557.77
	16.24	5.45	1.46	236.66	4664.95

Optical microscopy: The optical microscopy images for M and L thin films deposited on glasses substrate by the drop casting method shown in Figure.8. The micrograph of L image as a well-defined feather or needle shape also, shows that the M compound confirm the formation of malti- twin**.**

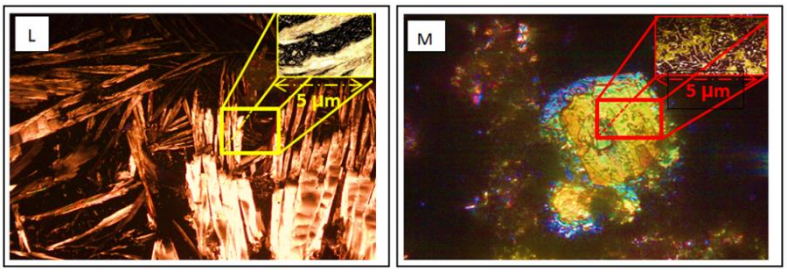

Figure.8. Optical microscopy images

Optical properties: The Transmittance spectrum is taken by Cary 100 Conc plus UV-Vis Spectrophotometer 300 nm to 900 nm. The UV-Vis spectra is very important because it provide the details related to the optical band. The spectra (L) show valley due to effect at UV range (300-360) nm, also the transmittance and absorption curves was subdivided into two regions at the visible region. The absorption curve decreases sharply from 360 nm up to 400 nm and after this wavelength tends to saturate, Figure.9a. The optical transmittance of the (M) thin film at was around 2% at wavelength 300 nm then increases sharply to 95% at wavelength 390 nm as shown in Figure.9b, So the (L and M) thin film have a good transmittance in the visible range, which can be used in solar cell and a smart window.

Figure.9c, shows the band gap of (L) thin film measured from the plot of $(\alpha h\upsilon)^2$ versus photon energy hυ. By extrapolating the linear part of the curve toward the photon energy axis, the band gap of (L) thin film was found to be 3.35 eV while Figure.9d, shows that the graph between $(\alpha h\nu)^2$ versus photon energy (hν) gives the value of direct band gap(where α is the absorption coefficient). The extrapolation of the straight line to $(\alpha h\nu)^2 = 0$, gives the value of the band gap. The energy gap was found to be 3.75eV .

Figure.9e, show the relation between the reflactin and the wavelength at the rang 300 nm to 900 nm for (L) thin film show tow peaks at the 300 nm to 400 nm, the first one which have 0.45 reflactane and other have the same reflactane, that mean a vibrational moving for the elements the composite (L).

The reflectance of (M) thin film increases from 0.26 to 0.58 when the wavelength increases from 300 nm to greater than 350 nm , Figure.9f. also the reflectance of (L,M), so rapidly decrease in reflaction at the range above 400 nm to 0.01. This measurement via to the thin films which prepared is smoth and homogeneous. The refractive index (n) is very similar to the reflacttion, Figure.9g,h. and has been calculated by the formula (1).

$$n = \frac{1+\sqrt{R}}{1-\sqrt{R}} \quad (1)$$

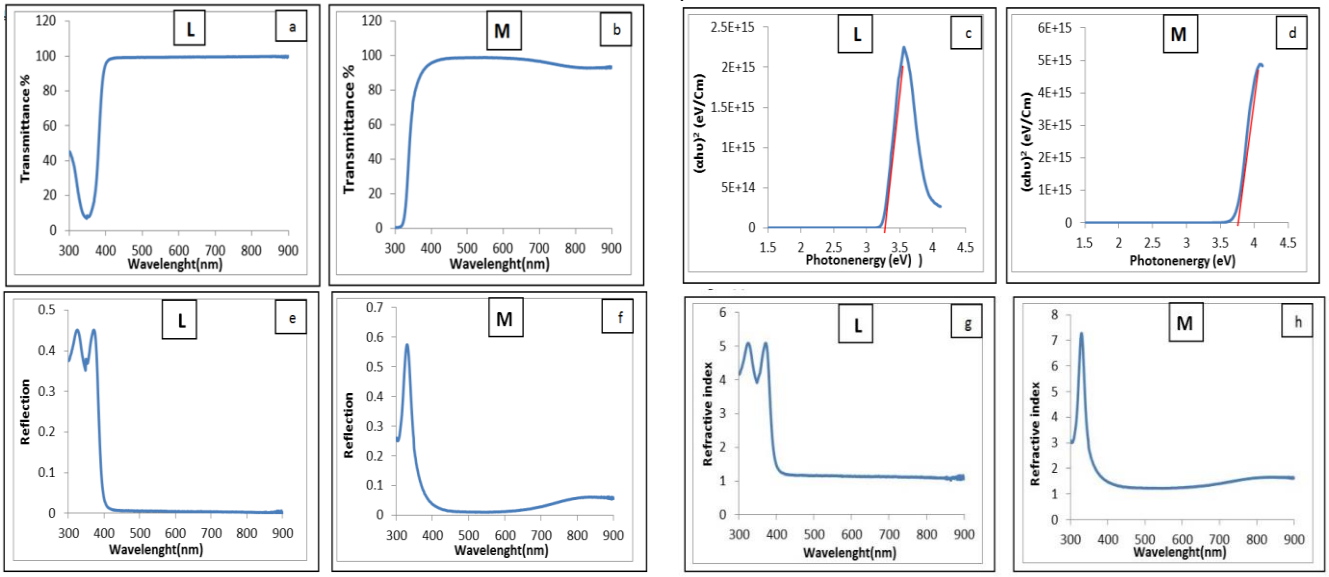

Figure.9. Optical properties (L and M)

Morphology study: The surface morphology of the synthesised (L and M) Nanoparticles were investigated by using AFM analysis.

Figure.10 reveals the (3-D) AFM images and the chart distribution of L and M thin films deposited on glass substrates. AFM image proves that the grains are uniformly distributed within the scanning area (500x500nm) with individual columnar grains extending upwards.

The average grins size of,pore is measured from AFM analysis using software and is found to be around 78 nm and 116 nm respectively depending on the preparation conditions (5 drop casting on glass substrates), Homogenous and a good roughness grain of L and M Nanostructure were noticed and listed in table.4.

Table.4. The grain size, Roughness and root mean square of (L and M)

Compound	Grain size (nm)	Roughens average (nm)	Root mean square (nm)
L	77.79	0.43	0.51
M	115.96	0.75	0.88

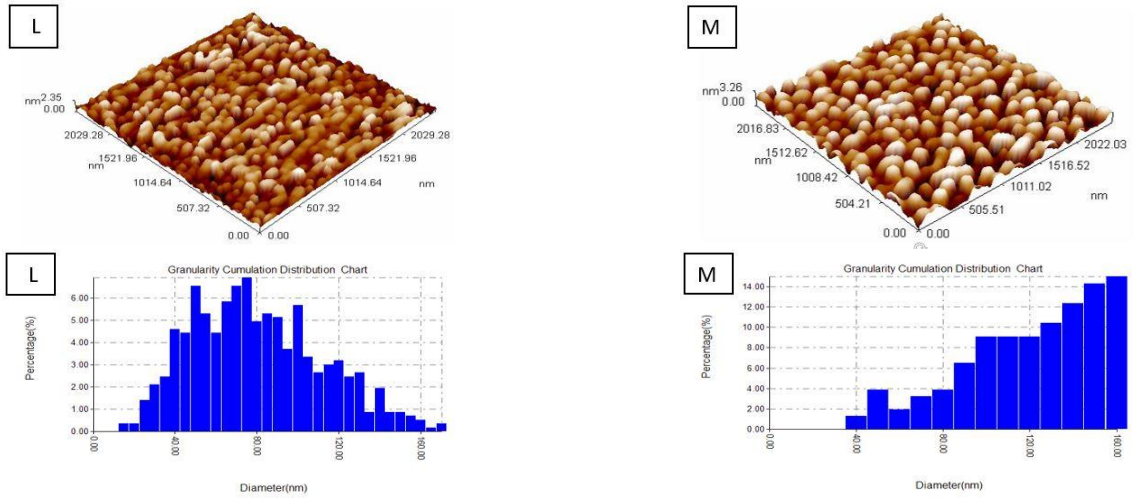

Figure.10. 3-D image and granularity cumulating distribution chart of (L and M)

L and M /Si Hetrojunction Solar cell properties: Figure.11 shows that the L and M particles are deposited on the surface silicon only five drops by the drop casting method then dry at 80^{o} C to faricate the solar cell L/Si and M/Si. I-V dark characteristics in forward and reverse direction of Al/L/p-Si/Al and Al/L/p-Si/Al solar cells. The forward current of Photodetector is very small at voltages less than 2 V. This current is known as recombination current which occurs at low voltages only. It is generated when each electron excited form valence band for the conductive band. The second region at high voltage represented the diffusion or binding region, which depending on serried resistance. In this region; the bias voltage can deliver electrons with enough energy to penetrate the barrier between the two sides of the junction.

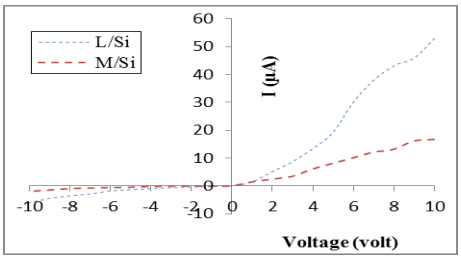

Figure.11. I-V characteristic under forward reverse bias of the L and M/ p-Si

Figure.12, shows that the reversed current-voltage characteristics of the device measured in dark and the photocurrent under a 40 W/ tungsten lamp illumination. It can be seen that the reverse current value at a given voltage for L/ p-Si hetetrojunction under illumination is higher than that in the dark and it can be seen from these figures that the current value at a given voltage for L/ p-Si under illumination is higher than that in M/p-Si this indicate that the light generated carrier – contributing photocurrent due to the production of electron –hole as a result of the light absorption. This behavior yield useful information on the electron-hole pairs, which are effectively generated in the junction by incident photons.

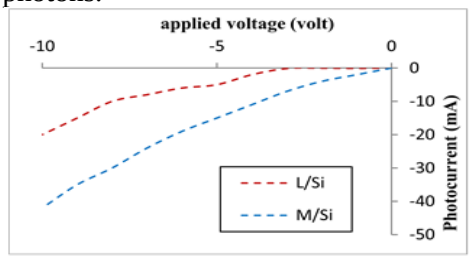

Figure.12 Illuminated (I-V) characteristic of L and M/p-Si solar cell

Figure.13, Shows the I-V characteristics for L/p-Si and M/p-Si heterojunction.The measured short- circuit current, open –circuit voltage, fill factor and Efficiency are (36.8 – 40.2) μA, (0.44-0.45) V, (40.46-40.24) and (6.55-7.28)% respectively. All the results relieve that the sandwich structure L/p-Si and M/p-Si could be used as a solar cell.

Table.5. Parameters of solar cell

Compound	Voc	Isc	Vm	Im	f.f	eff
L	0.44	36.8	0.28	23.4	40.46	6.55
M	0.45	40.2	0.28	26	40.24	7.28

Figure.13. I-V characteristics for solar cell with illumination, for L/p-Si and M/p-Si

4 CONCLUSION

The synthesised L and M NPS were in nanosized 50 nm prepared in ethanol by Chemical method and the optical properties revealed that the direct band gap of L and M NPS indicated to the effect of quantum size. X-ray diffraction (XRD) measurement disclosed that the L and M NPS are polycrystalline structure and no other phases were noticed, Deposition of L and M NPS on silicon (p-Si) gave suspensions solar cell characteristics enhanced the properties solar cells.

REFERENCES

Abd A.N, Improved photoresponse of porous silicon photodetectors by embedding CdS nanoparticles, World Scientific News, 19, 2015, 32–49.

Abid K.K, Al Bayati R.H and Faeq A.A, Transition Metal Complexes of New N-Amino Quinolone Derivative, Synthesis, Characterization, Thermal Study and Antimicrobial Properties, 6 (2), 2016, 29–35.

Alaghaz A.M.A, Bayoumi H.A, Ammar Y.A and Aldhlmani S.A, Synthesis, characterization and antipathogenic studies of some transition metal complexes with N, O-chelating Schiff's base ligand incorporating azo and sulfonamide Moieties H 2 N S, J. Mol. Struct., 1035, 2013, 383–399.

Ali A, Cheow S.L, Azhari A.W, Sopian K and Zaidi S.H, Results in Physics Enhancing crystalline silicon solar cell efficiency with Si x Ge 1 A x layers, Results Phys., 2016.

Huang Y, Effects of Electronic Structure and Interfacial Interaction between Metal-quinoline Complexes and TiO_2 on Visible Light Photocatalytic Activity of TiO_2, Applied Catal. B, Environ., 2016.

Jayamani A, Thamilarasan V and Sengottuvelan N, Spectrochimica Acta Part A, Molecular and Biomolecular Spectroscopy Synthesis of mononuclear copper (II) complexes of acyclic Schiff's base ligands, Spectral, structural, electrochemical, antibacterial, DNA binding and cleavage activity, Spectrochim. ACTA Part A, Mol. Biomol. Spectrosc., 122, 2014, 365–374.

Jennifer F, Synthesis, Antimicrobial and Anti-Inflammatory studies of some novel Schiff Base Derivatives, Int. J. Drug Dev. & Res., 6 (2), 2014, 165–171.

Kumar A, Fernandes J and Kumar P, Synthesis And Biological Evaluation Of Some Novel Isoxazoline Derivatives of Carbostyril, WJPPS, 3 (2), 2014, 1267–1277.

Luo C.Z, Gandeepan P, Wu Y.C, Chen W.C and Cheng C.H, Copper promoted synthesis of substituted quinolines from benzylic azides and alkynes, RSC Adv., 5 (128), 2015, 106012–106018.

Majeed A.M.A, Abd A.N, Hussein A.A and Habubi N.F, Fabrication and Characterization of Copper Oxide Nanoparticles / PSi Heterodiode, International Letters of Chemistry, Physics and Astronomy, 57, 2015, 25–35.

Shakya P.R, Singh A.K and Rao T.R, Synthesis and characterization of lanthanide (III) complexes with a mesogenic Schiff-base, N, N′-di-(4-decyloxysalicylidene)-2′,6′- diaminopyridine, Mater. Sci. Eng. C, 32 (7), 2012, 1906–1911.

Shebl M, Spectrochimica Acta Part A : Molecular and Biomolecular Spectroscopy Synthesis, spectroscopic characterization and antimicrobial activity of binuclear metal complexes of a new asymmetrical Schiff base ligand, DNA binding affinity of copper (II) comple, Spectrochim, Acta Part A Mol. Biomol Spectrosc., 117, 2014, 127–137.

Tyagi M, Chandra S and Tyagi P, Spectrochimica Acta Part A, Molecular and Biomolecular Spectroscopy Mn (II) and Cu (II) complexes of a bidentate Schiff's base ligand, Spectral, thermal, molecular modelling and mycological studies, Spectrochim. ACTA PART A Mol. Biomol. Spectrosc., 117, 2014, 1–8.

Witaicenis A, Phytomedicine Antioxidant and intestinal anti-inflammatory effects of plant-derived coumarin derivatives, Eur. J. Integr. Med., 21 (3), 2014, 240–246.

Xi G and Liu Z, Coumarin-Fused Coumarin, Antioxidant Story from, 2015.

Zheng Z, Efficient Charge Transfer and Fine-Tuned Energy Level Alignment in a THF-Processed Fullerene-Free Organic Solar Cell with 11.3 % Efficiency, Materials Views, 2016, 3–8.